Chapter 7

Dielectric and Mechanical properties of Sn doped $CaCu_3Ti_4O_{12}$/ Poly(vinylidene fluoride) Composites

The present chapter describes the structural, dielectric and mechanical properties of Sn doped $CaCu_3Ti_4O_{12}$ / PVDF composites. Sn doped $CaCu_3Ti_4O_{12}$ (SnCCTO) has been prepared by solid state ceramic method. It is observed that Sn doping in $CaCu_3Ti_4O_{12}$ enhances its dielectric permittivity and decreases the dielectric loss. PVDF/SnCCTO (PVDF-SnC) composites have been prepared by melt extrusion method. It has been found that SnCCTO dispersion proves to be an effective method in improving the thermal, dielectric and mechanical properties of PVDF.

7. Results and discussion

7.1. Structural Analysis

X-ray diffraction patterns of SnCCTO, PVDF and composites containing 10, 20 and 50 wt % SnCCTO (PVDF-SnC) are shown in fig 7.1. Formation of the single phase solid solution in SnCCTO is confirmed by powder X-ray diffraction (XRD) using CuKα radiation. In the case of SnCCTO, the diffraction peaks corresponding to the reflections (220), (310), (222), (321), (400), (422) and (440) are observed at 2θ values of 34.2°, 38.5°, 42.3°, 45.8°, 49.2°, 61.3° and 72.2° respectively. This confirms the formation of single phase [Sinclair et al (2002)]. There is no evidence of presence of any secondary phase in SnCCTO. Lattice parameter "a" increases from 7.3907 A (for CCTO) to 7.3929 for SnCCTO.

α- PVDF has been used in the present work (as supplied). This is proved by its characteristic 2θ peaks at 17.7°, 18.7°and 19.9° corresponding to (100), (020) and (110) reflections respectively [Varma et al (2010)]. Intensity of three major peaks (220), (400) and (422) of SnCCTO in the composites increases with its increasing amount. Predominance of SnCCTO phase can be seen in PVDF-50SnC. This is indicated by the suppression of the peaks of PVDF. In SnCCTO, (220), (400) and (422) peaks are present

at 34.2°, 49.2° and 61.3° which shift to 34.7°, 49.7° and 61.8° respectively in the case of PVDF-50SnC. This shift in the peaks towards higher 2θ values is due to a decrease in the interplanar spacing. Compression of SnCCTO particles by PVDF matrix seems to decrease the interplanar spacing.

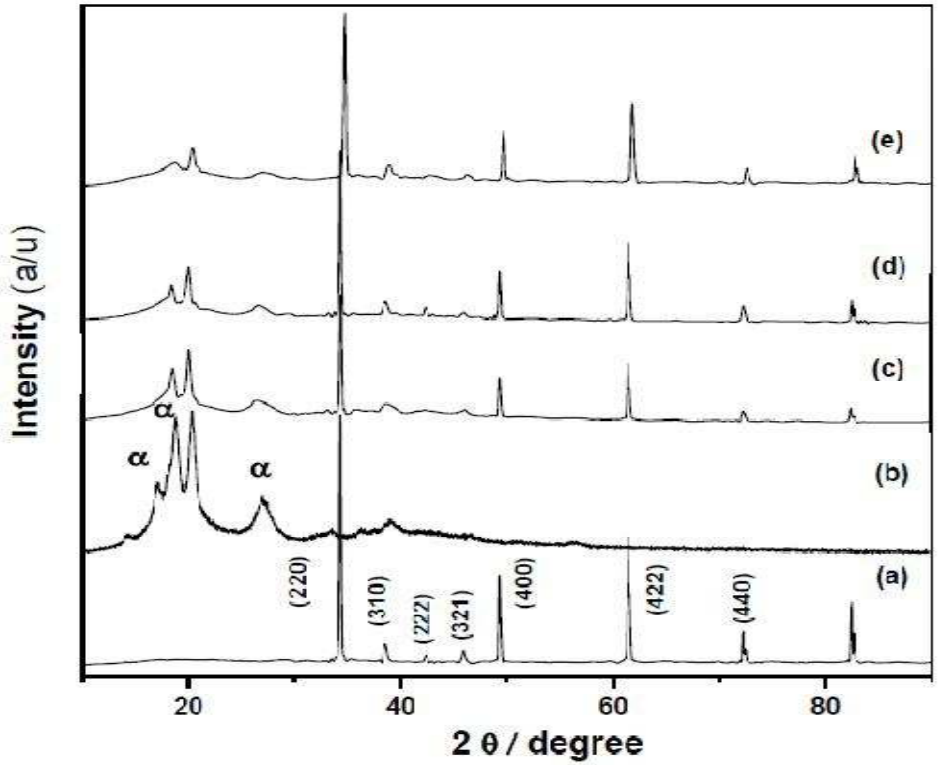

Figure 7.1 X-ray diffraction patterns for (a) SnCCTO, (b) PVDF, (c) PVDF-10SnC, (d) PVDF-20SnC and (e) PVDF-50SnC composites

7.2. Surface morphology

Distribution of ceramic particles in the polymer matrix plays an important role in determining the properties of the composite materials. Figure 7.2 shows SEM micrographs of PVDF and the composites. Pure PVDF exhibits spherulitic morphology. It is observed that the spherulitic morphology of pure PVDF is significantly changed by dispersion of SnCCTO powder. Figure 7.2 shows that the ceramic particles are well dispersed in the polymer matrix for low concentration of SnCCTO. As the filler

concentration increases, the inter - particle distance decreases, leading to the formation of a connected network structure. This is evident from the SEM micrograph of the PVDF-50SnC composite. These changes in the morphology of the composites influence the properties. This well connected network structure in PVDF-50SnC gives rise to an enhanced ε' and improves the mechanical properties as described below.

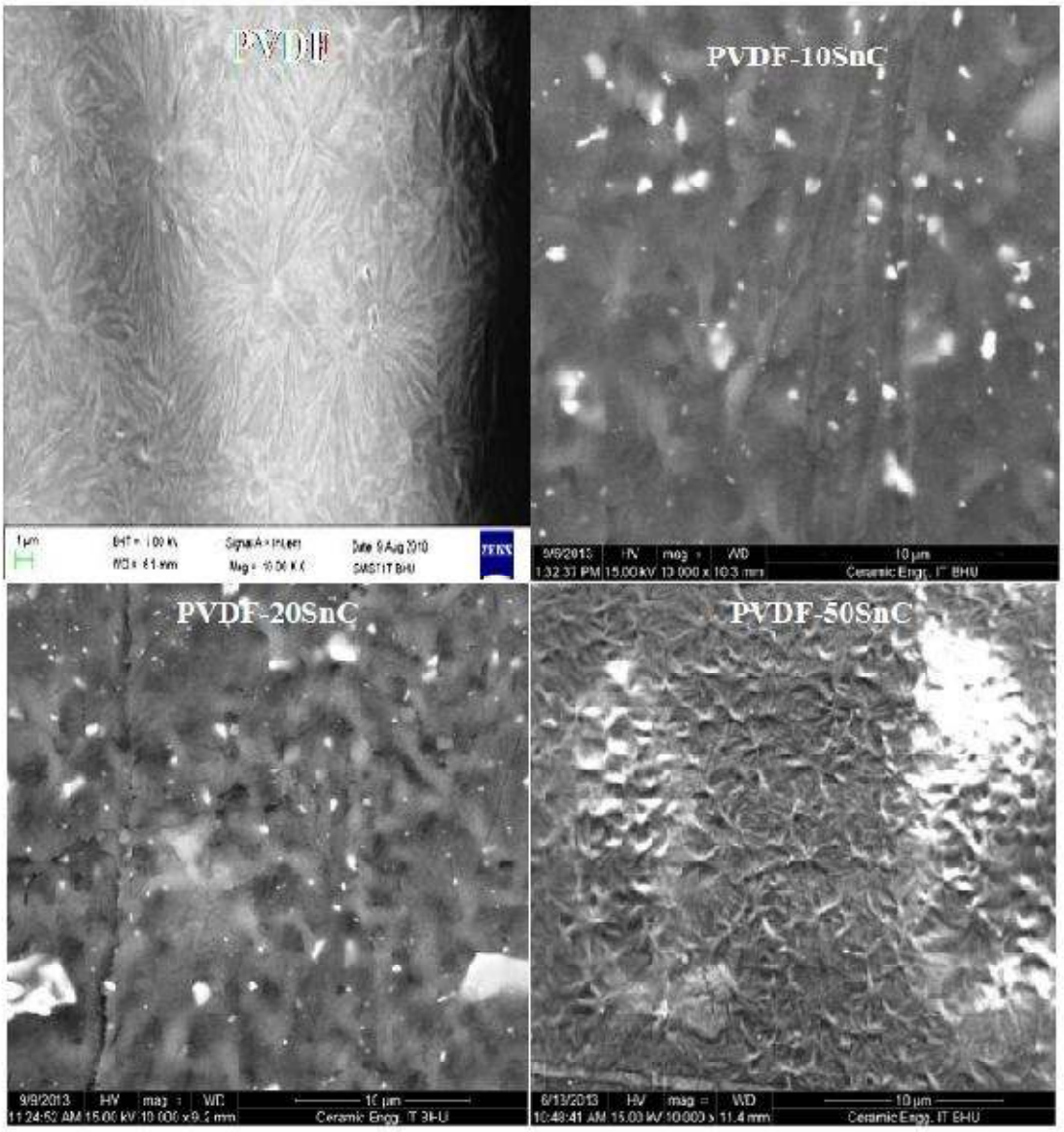

Figure 7.2 Scanning electron micrographs of PVDF, PVDF-10SnC, PVDF-20SnC and PVDF-50SnC composites.

7.3 Thermal behavior

Thermogravimetric analysis (TGA) has been carried out to study the thermal stability of the polymer and the composites. Thermograms recorded for the pure PVDF and its composites are shown in Fig 7.3. It is observed that pure PVDF is stable up to 400°C and complete degradation of the polymer occurs at around 500°C. Addition of SnCCTO ceramic filler influences the thermal decomposition behavior of PVDF polymer. SnCCTO filler shifts the degradation temperature to higher side i.e. from 442^0C in PVDF to 444^0C, 458^0C and 475^0C in PVDF-10SnC, PVDF-20SnC and PVDF-50SnC respectively. It shows that SnCCTO dispersion improves the thermal stability of the composites.

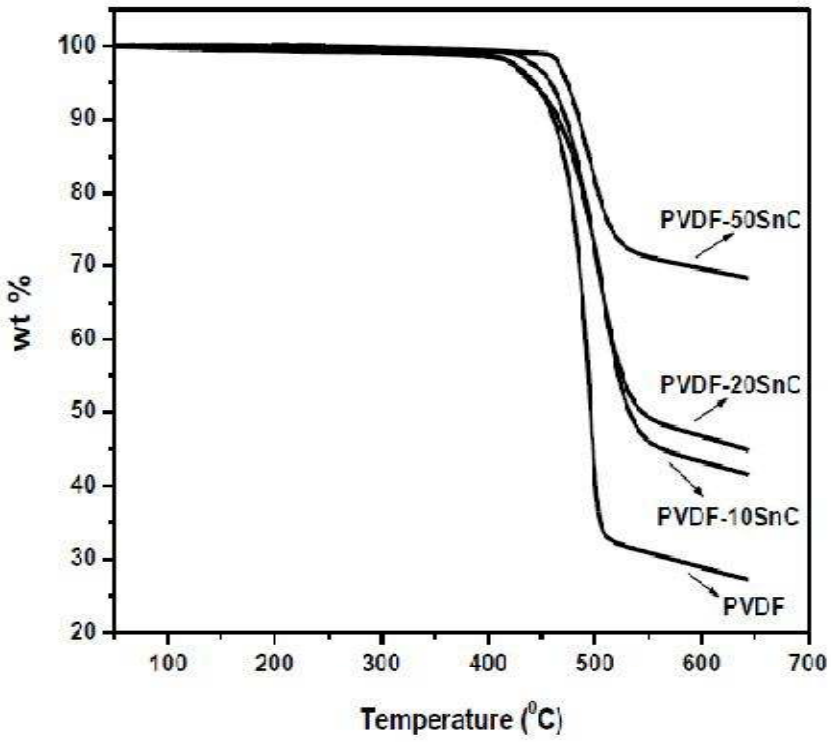

Figure 7.3 TGA of pure PVDF, PVDF-10SnC, PVDF-20SnC and PVDF-50SnC composites.

7.4. Mechanical properties

Figure 7.4 (a) shows the stress-strain curves of PVDF and its composites. Considerable increase is observed in the value of Young's modulus which is calculated

from the slope of the linear region of the plots. For PVDF, PVDF-10SnC, PVDF-20SnC and PVDF-50SnC, the values of Young modulus are 750, 760, 840, 1020 MPa, respectively (Fig 7.4 b). Elongation at breaking point decreases from 30% in PVDF to 21%, 18% and 16% in PVDF-10SnC, PVDF-20SnC and PVDF-50SnC composites respectively (Fig 7.4 c).This increase in the Young's modulus with filler content can be attributed to the increase in the resistance to the free movement of the polymeric chains by much harder ceramic particles. This also explains the observed decrease in the elongation at the breaking point with increasing concentration of ceramic in the PVDF matrix.

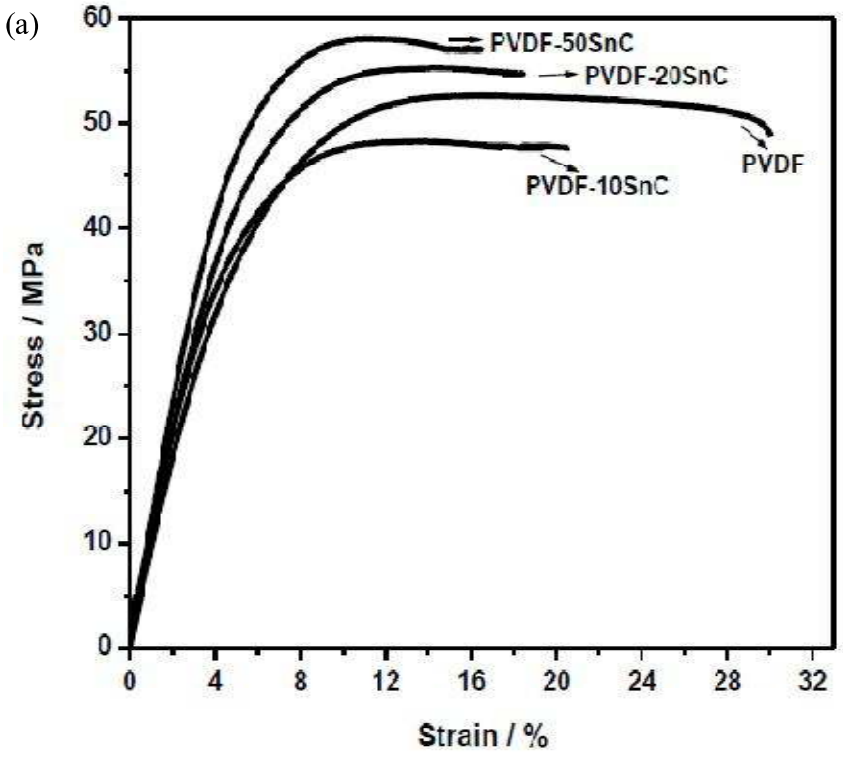

Figure 7.4 (a) Stress-strain curves for pure PVDF, PVDF-10SnC, PVDF-20SnC and PVDF-50SnC composites.

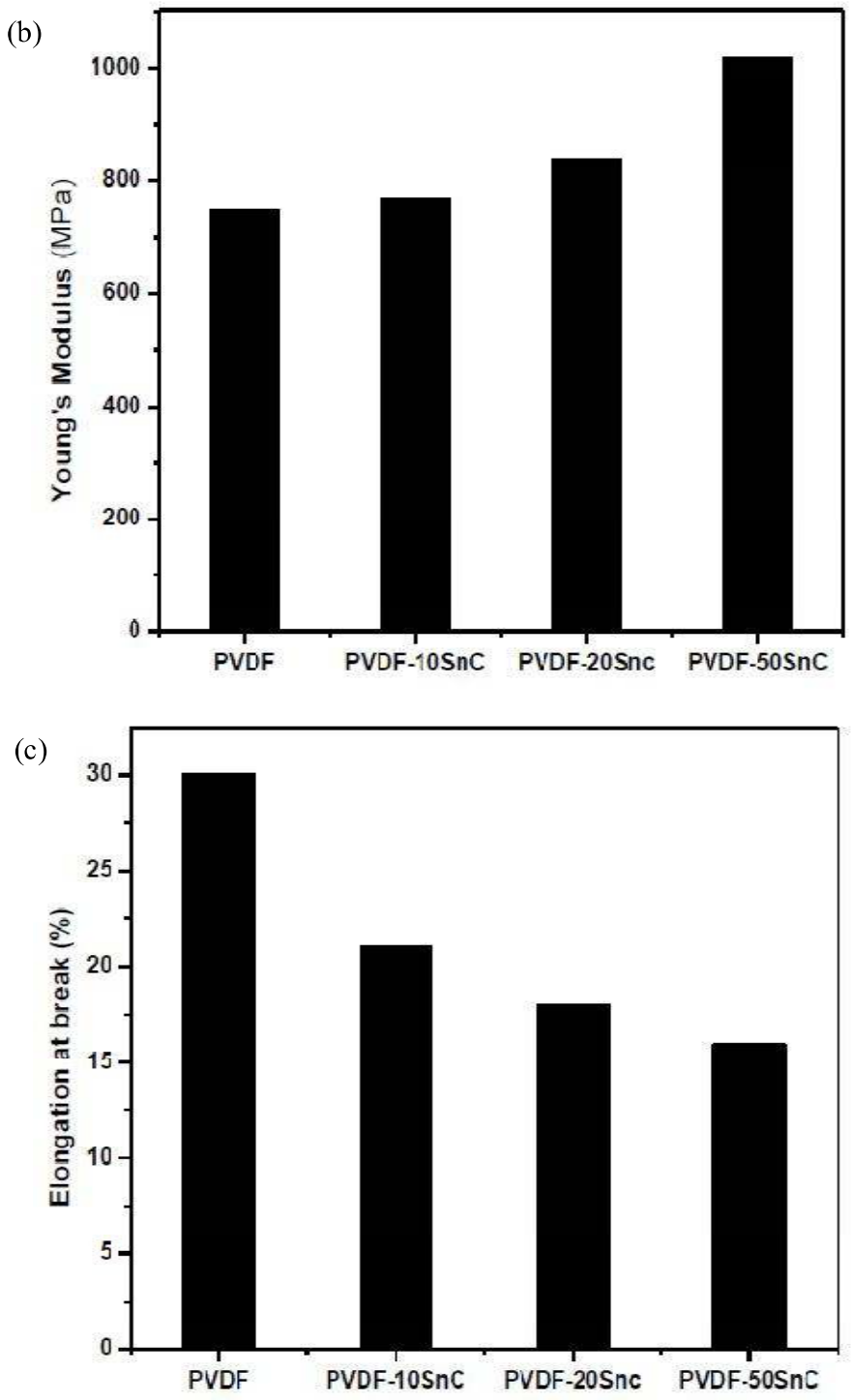

Figure 7.4 (b) Young's modulus of PVDF and composites and (c) Elongation at breaking point of PVDF and composites.

7.5. Dielectric properties

Frequency dependence of dielectric permittivity of CCTO and SnCCTO is shown in fig 7.5 (a). The dielectric permittivity of CCTO is 3100 at 40^{o}C and 100 Hz. On doping with Sn, it increases to 7050 at 40^{o}C and 100 Hz. CCTO and SnCCTO have frequency independent ε' in the frequency range 1-10^{6} Hz. High value of the dielectric permittivity in CCTO and SnCCTO has been explained due to the formation of barrier layers at grains – grains boundaries interfaces. This gives rise to interfacial polarization [Sinclair et al (2002)]. Interfacial polarization arises whenever there is a difference in the conductivity of two or more phases which are in electrical contact with each other (PVDF and SnCCTO in this case).

ε' increases with temperature in PVDF and one relaxation appears around 10^{4} Hz at 40^{0}C (Fig 7.5 c). Dielectric permittivity increases with increasing content of SnCCTO in PVDF (Fig 7.5 e). The dielectric permittivity at 100 Hz and 40°C for PVDF, PVDF-10SnC, PVDF-20SnC and PVDF-50SnC is 3, 26, 32 and 77, respectively. PVDF is present in α phase, which is non-polar. Due to the non-polar nature of PVDF, the value of ε' is low. The dielectric permittivity for the composites is more than that of pure PVDF. Increase in the dielectric permittivity with increasing ceramic content can be explained as follows. High dielectric permittivity of the composites is mainly because of the interfacial polarization and the high dielectric permittivity of SnCCTO. In the polymers matrix composites, interfacial polarization is always present due to existence of heterogeneities (multiphase systems), in the system. Interfacial polarization arises due to the difference in the conductivity of the phases which are in electrical contact with each other (PVDF and SnCCTO in the present case). Its contribution increases with increase in the interfacial area between the phases. Increase in the interfacial area with increasing content of SnCCTO in PVDF enhances the interfacial polarization and hence the dielectric permittivity. Since interfacial polarization involves movement of charges over long distances, therefore, it relaxes in the low frequency range i.e. the dipoles cannot follow the alteration of the applied field at high frequencies. Therefore, the value of dielectric permittivity and dielectric loss is high at low frequency and decreases rapidly with

increase in frequency. Variation of ε' with frequency at a few temperatures for all the compositions is shown in figs 7.5 (c, g, i and k). Initially a rapid decrease in ε' with frequency in the low frequency region is followed by a plateau above a certain frequency. It is clear from the figure 7.5 (e), that ε' does not depend much on the frequency in the range 10^2-10^6 Hz. It is a desirable characteristic for electronics devices.

Tan δ vs log f (frequency) plots of CCTO, SnCCTO, PVDF and PVDF-SnC composites are shown in Figs 7.5 (b, d, f, h, j and l). Dielectric loss (tan δ) decreases with Sn doping in CCTO from 0.86 (in CCTO) to 0.32 (in SnCCTO) at 100 Hz and 40°C. In CCTO one relaxation appears at low frequency and other at intermediate frequency. It seems that on Sn doping both the relaxation shift towards higher frequency in SnCCTO. The higher frequency relaxation in SnCCTO seems to occur beyond the frequency range of the instrument.

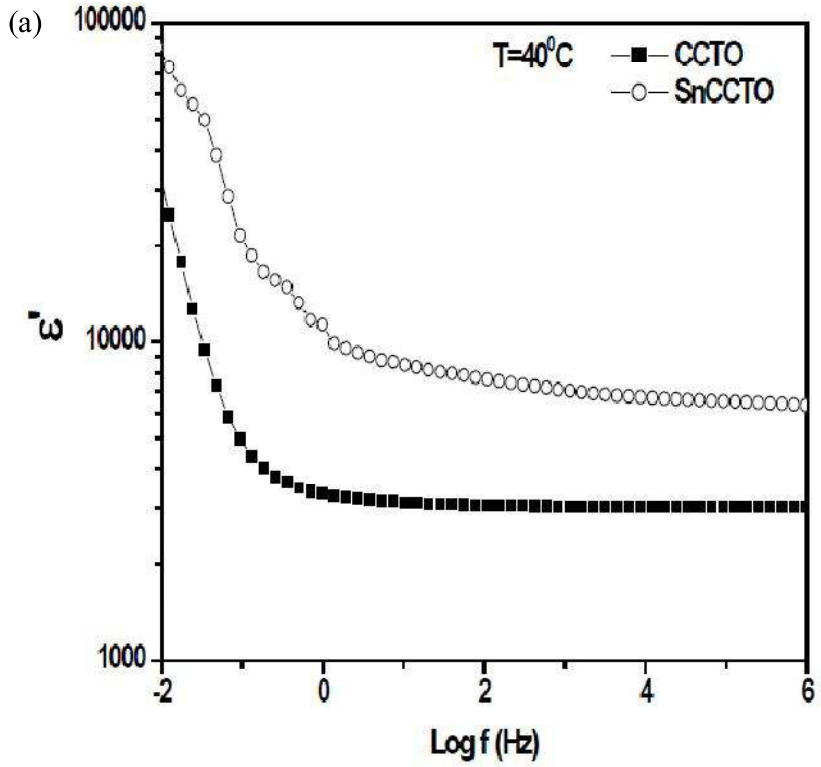

Figure 7.5 (a) Frequency dependence of dielectric permittivity of CCTO and SnCCTO at 40^0C.

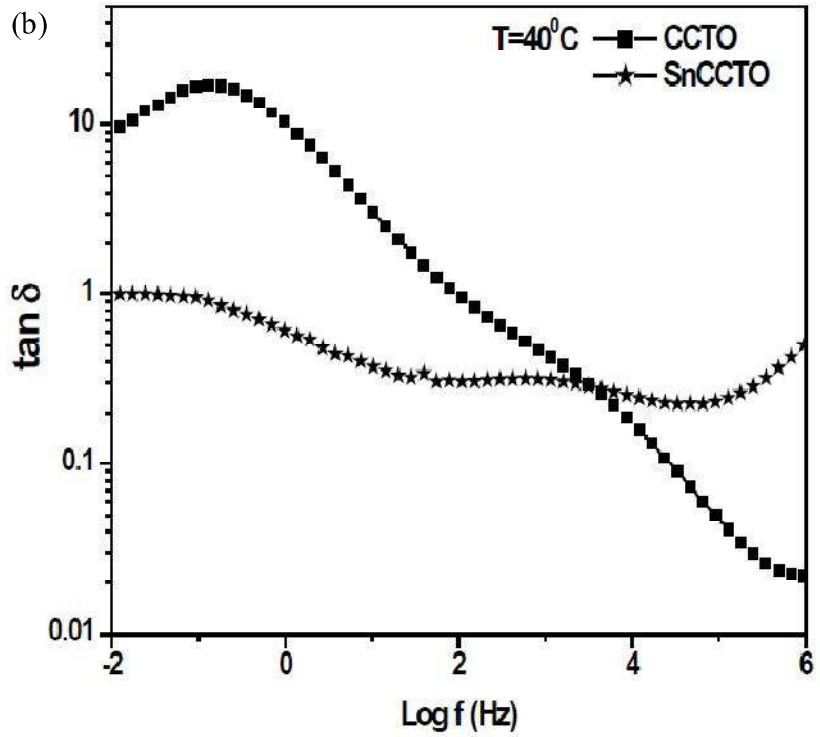

Figure 7.5 (b) Frequency dependence of tan δ of CCTO and SnCCTO at 40^0C.

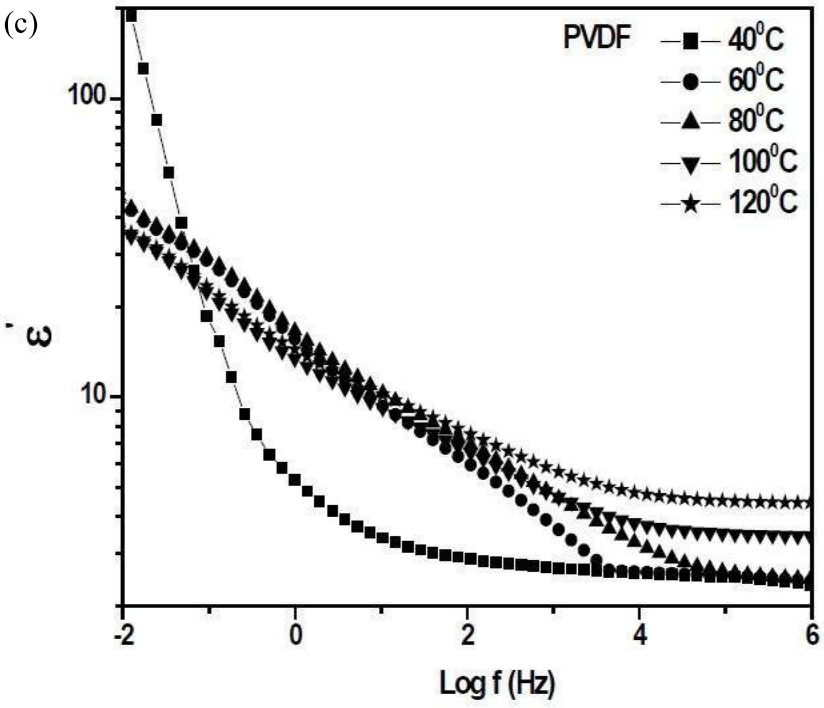

Figure 7.5 (c) Frequency dependence of dielectric permittivity PVDF at different temperatures.

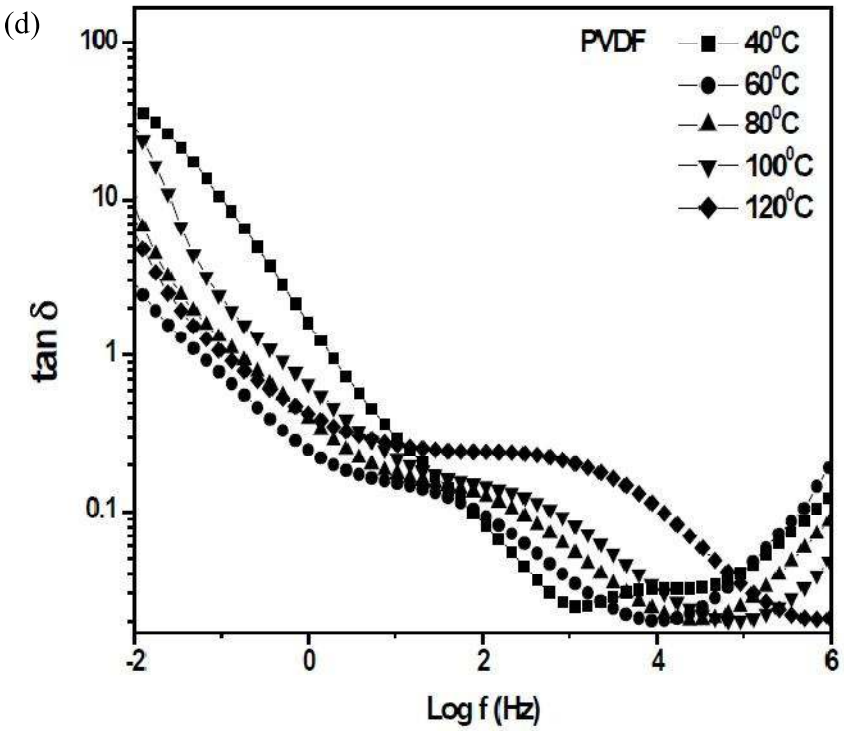

Figure 7.5 (d) Frequency dependence of tan δ of PVDF at different temperatures.

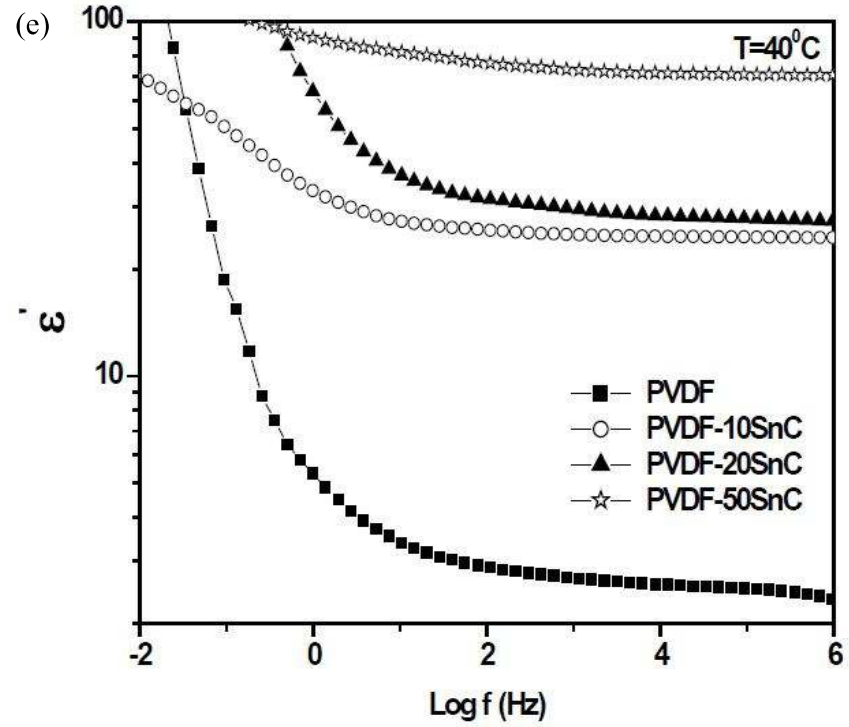

Figure 7.5 (e) Frequency dependence of dielectric permittivity PVDF and all the composites at 40^0 C.

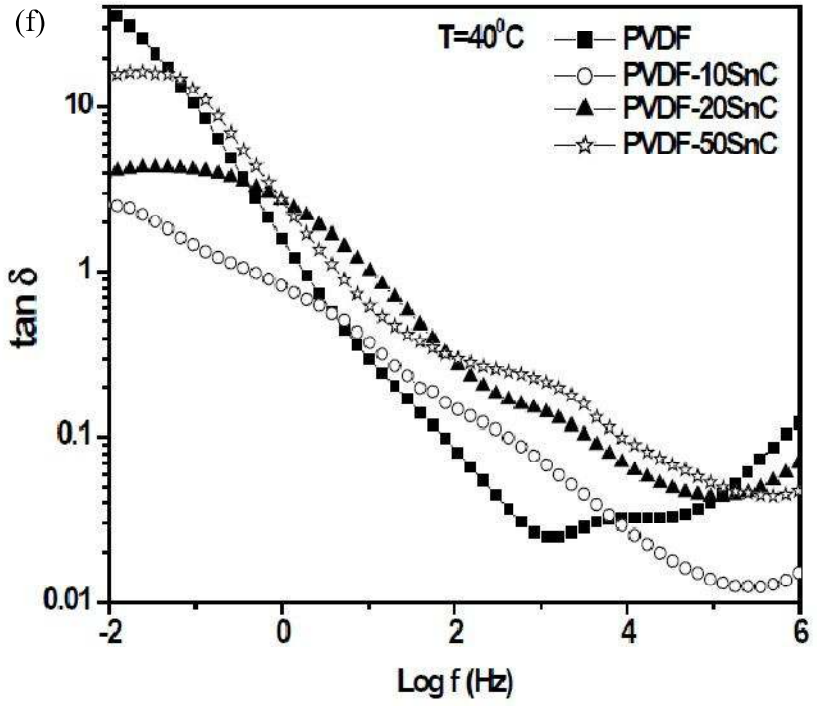

Figure 7.5 (f) Frequency dependence of tan δ of PVDF and all the composites at 40^0 C.

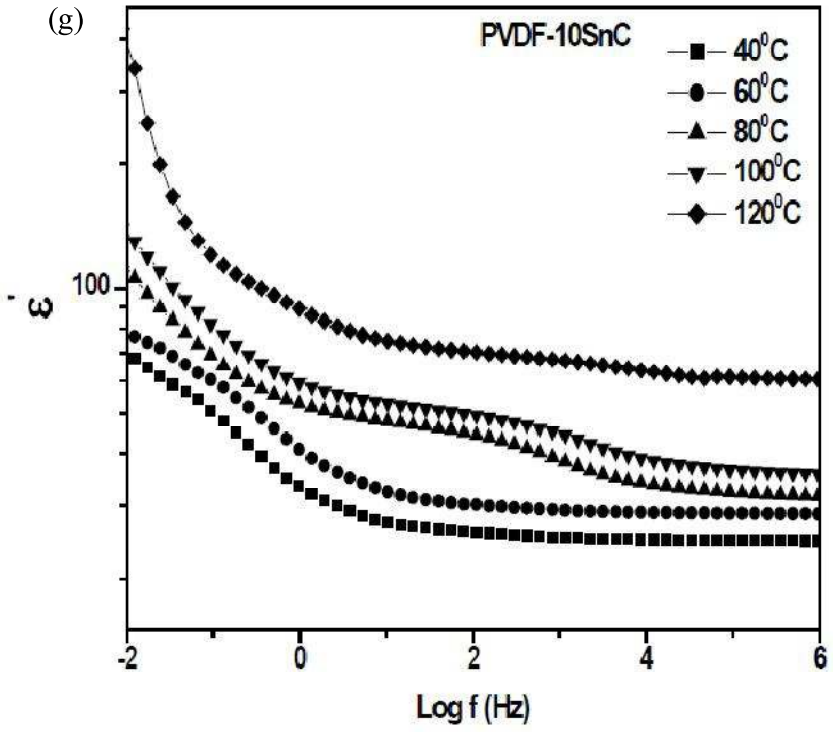

Figure 7.5 (g) Frequency dependence of dielectric permittivity PVDF-10SnC at different temperatures

(h)

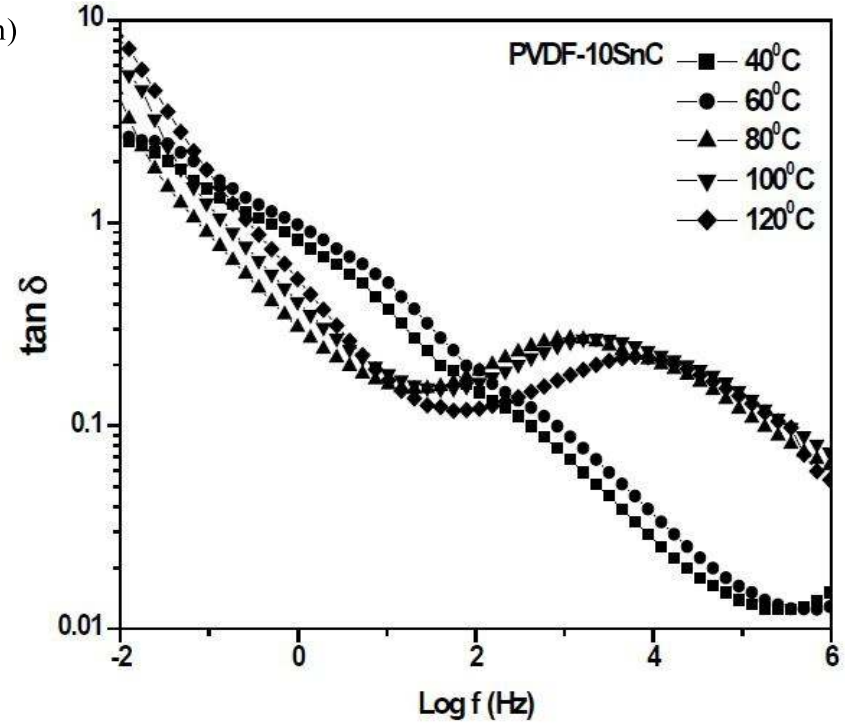

Figure 7.5 (h) Frequency dependence of tan δ of PVDF-10SnC at different temperatures.

(i)

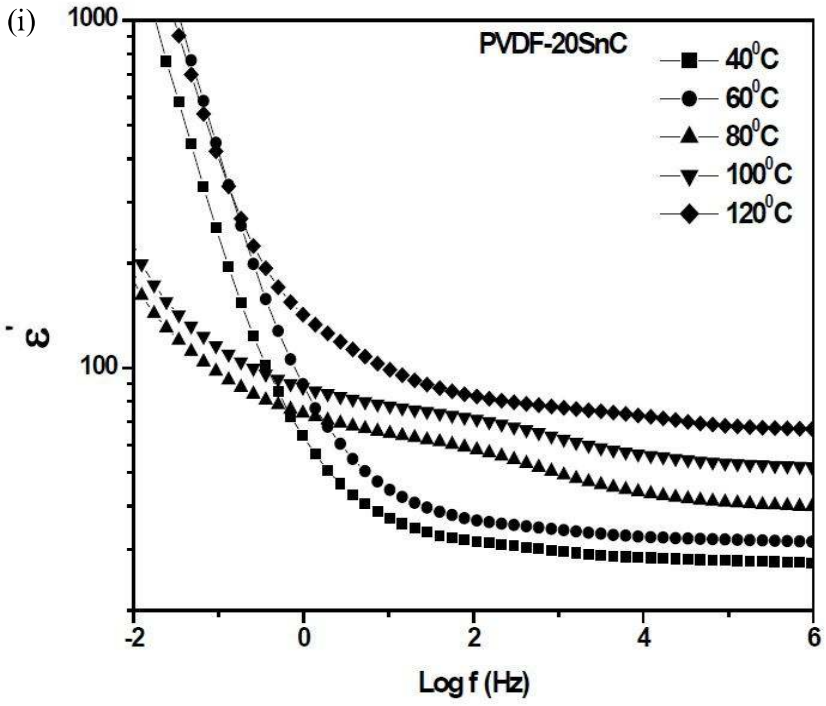

Figure 7.5 (i) Frequency dependence of dielectric permittivity PVDF-20SnC at different temperatures.

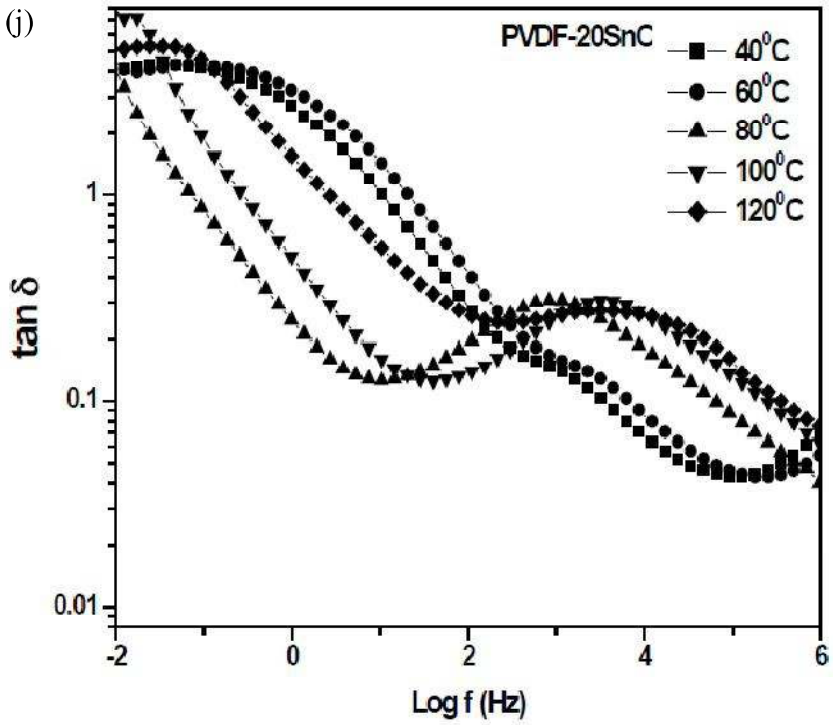

Figure 7.5 (j) Frequency dependence of tan δ of PVDF-20SnC at different temperatures.

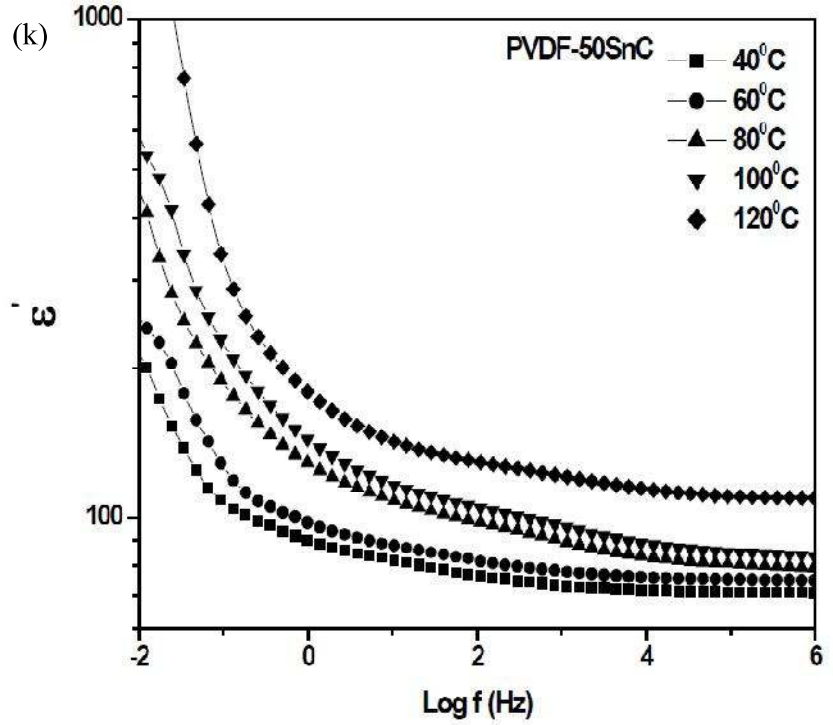

Figure 7.5 (k) Frequency dependence of dielectric permittivity PVDF-50SnC at different temperatures.

(l)

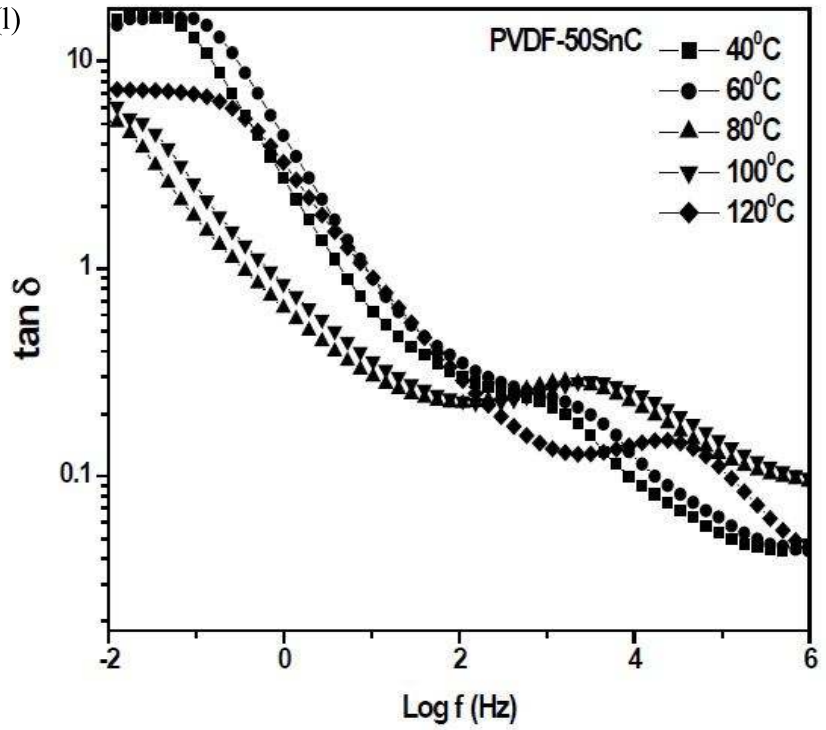

Figure 7.5 (l) Frequency dependence of tan δ of PVDF-50SnC at different temperatures.

Values of the dielectric loss at 100 Hz and 40°C for PVDF, PVDF-10SnC, PVDF-20SnC and PVDF-50SnC are 0.09, 0.15, 0.26 and 0.29 respectively (Fig f). In the case of composites, two dielectric relaxations are observed (Figs 7.5 h, j and l). One dielectric relaxation appears in the frequency range 10^2 -10^4 Hz, while other in the low frequency range, 10^{-1}-10^1 Hz. The frequency of this relaxation shifts to lower side with increasing concentration of SnCCTO. In composites at 40^0C and 60^0C one relaxation appears at low frequency 0-10 Hz, while the other occurs at intermediate frequency 100 Hz-10 KHz. Relaxation at lower frequency can be attributed to Maxwell Wagner polarization in the composites and the one in the intermediate frequency range can be attributed to α_c relaxation associated with molecular motion of the polymer chains in the crystalline regions of PVDF. The glass transition relaxation α_a of PVDF occurs beyond 1 MHz (Fig 4.5 d) [Gregoria and Cestari (1994); Gregoria and Ueno (1999); Channel and Jog (2008)]. With increase in temperature both these relaxation shifts to higher frequency side. In the composites above 60^0C, the α_c relaxation associated with molecular motion of the polymer chains in the crystalline regions of PVDF [Thomas et al (2010); Chiang et al

(2001); McCrum et al (1967)] shifts to much higher frequency which could not be measured due to limited range of frequency measurement available in our system. This indicates that relaxation time decreases with increase in temperature due to ease of relaxation at higher temperature.

To understand the nature of dielectric relaxation modulus spectroscopy has also been used. Electrical modulus is defined as the inverse of complex permittivity.

$$M^* = \frac{1}{\varepsilon^*} = \frac{1}{(\varepsilon' - J\varepsilon'')} = \frac{\varepsilon'}{(\varepsilon'^2 + \varepsilon''^2)} + \frac{J\varepsilon''}{(\varepsilon'^2 + \varepsilon''^2)} = M' + J.M'' \qquad (7.1)$$

where M', ε' and M", ε" are the real and imaginary parts of the modulus and permittivity respectively. The real M' and imaginary M" parts of electrical modulus were obtained as a function of frequency [Ramajo et al (2008)]. It is observed from the figure 7.6 (a) that for PVDF and composites, there is a steep rise in the value of M' at a particular frequency. This frequency decreases with increasing content of SnCCTO. This corresponds to a dielectric relaxation. A corresponding peak is observed in the M" vs log f plot at the same frequency (fig 7.7 c). This corresponds to the dielectric relaxation process observed in M' vs log f plots. This relaxation is also observed in PVDF (fig 7.7 b). Height of this peak decreases with increasing concentration of SnCCTO. With the increase in SnCCTO content this relaxation peak shifts to lower frequency side in the composites. This is due to restricted mobility of the polymeric chains because of their interaction with the filler particles. This shows that the dielectric permittivity as well as the dielectric loss increases with increasing concentration of SnCCTO. The relaxation frequency shifts to higher side with increasing temperature (Figs 7.6 d-f). This relaxation is due to α_c relaxation associated with molecular motion of the polymer chains in the crystalline regions of PVDF.

Figures 7.6 (d-f) show variation of M" vs log f for PVDF-SnC composites at different temperatures. It is observed that another peak appears at low frequency at high temperature (above 60^{o}C). This peak shifts to higher frequency with increasing

temperature. This peak is not observed at 40°C and 60°C, as it is present at much lower frequency. It is not observed in PVDF also. Therefore, this relaxation is of Maxwell-Wagner-Sillar (MWS) type [Ramajo et al (2008); Hedvig (1977)]. Maxwell Wagner Sillar polarization is always present in the multiphase systems having phases with different conductivities i.e. electrical heterogeneities. In such materials, the charge accumulates at the ceramic particles - polymer interface. This gives rise to space charge polarization, which gives high value of dielectric permittivity as well as the dielectric loss. As the dielectric permittivity of SnCCTO is much higher than that of PVDF matrix, unbounded charges form the large dipoles at the polymer matrix – ceramic interface. These induced dipoles find it difficult to follow the alternation of the electric field and thus the resulting relaxation process occurs in the low frequency region or at high temperatures.

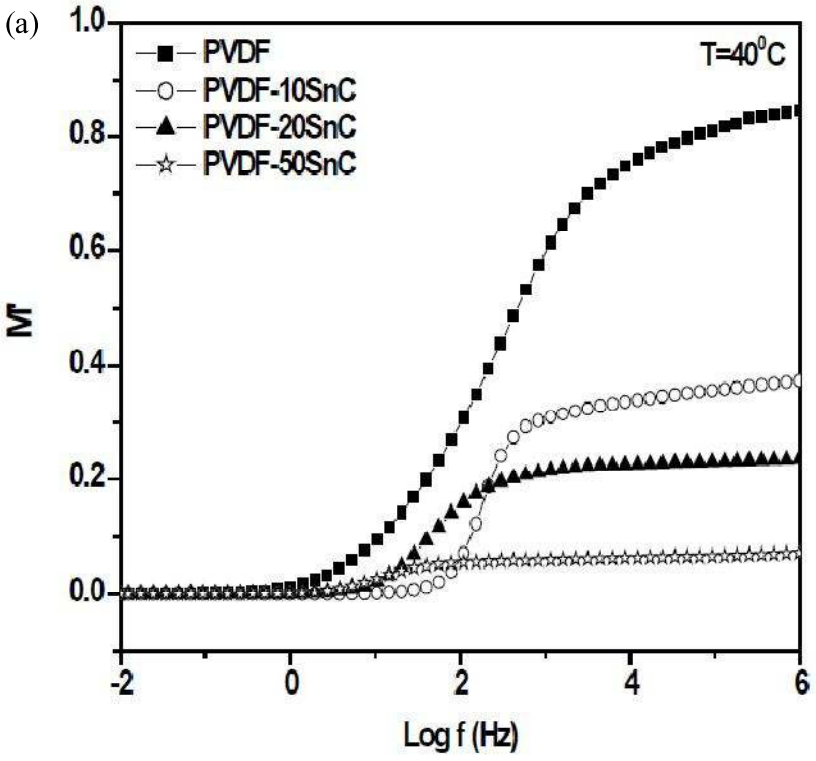

Figure 7.6 (a) M' vs log f plots of PVDF and composites at 40° C.

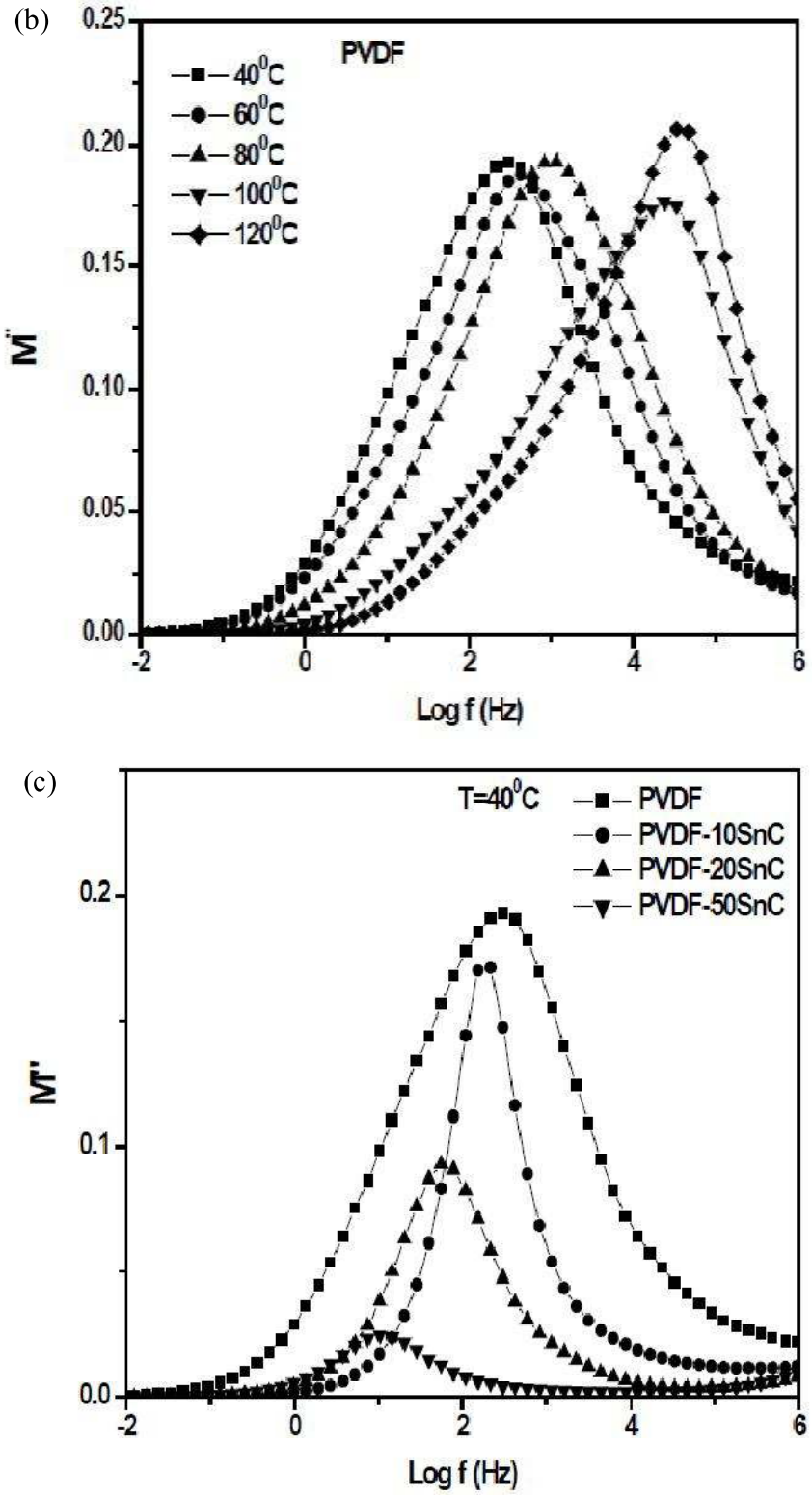

Figure 7.6 M" vs log f plots of (b) PVDF at different temperatures, (c) PVDF and PVDF-SnC composites at 40^0C

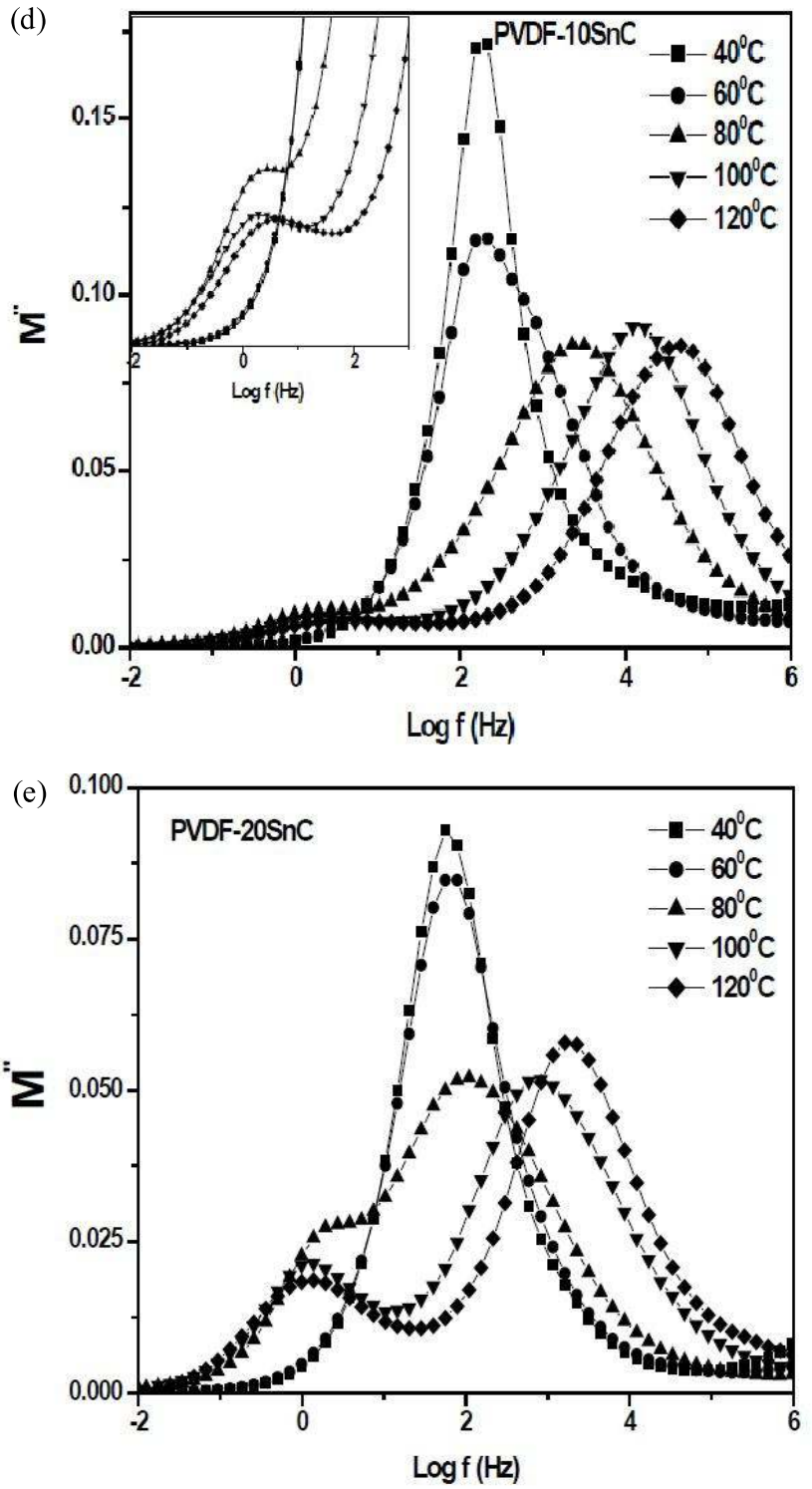

Figure 7.6 M" vs log f plots of (d) PVDF-10SnC at different temperatures, (e) PVDF-20SnC at different temperatures

(f)

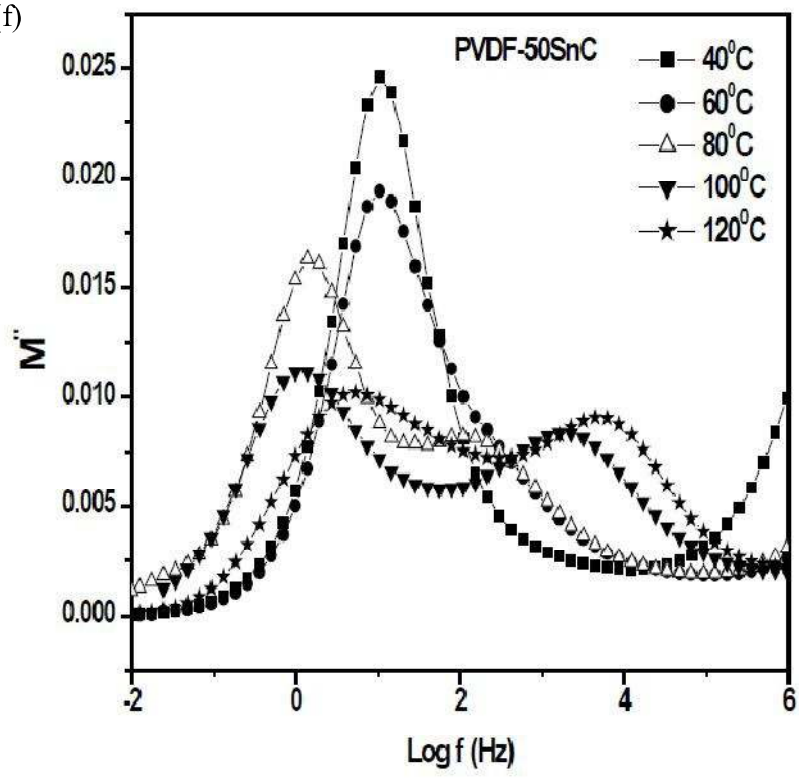

Figure 7.6 M" vs log f plots of (f) PVDF-50SnC at different temperatures.

Relaxation times, τ was determined using the relation $\tau = \frac{1}{2\pi f}$ where f is the frequency in cycles per second at the peak position in M" vs log f plots. Plots of log τ vs 1000/T for SnCCTO, PVDF, PVDF-10SnC, PVDF-20SnC and PVDF-50SnC are shown in fig 7.7. These plots are linear in accordance with Arrhenius relationship given below.

$$\tau_{max} = \tau_o \exp(\frac{E_R}{kT}) \qquad (7.2)$$

where E_R is the activation energy associated with the relaxation process, τ_o the pre-exponential factor, k is the Boltzmann constant and T is the absolute temperature. Values of activation energy obtained from the slopes of these linear plots are given in Table 7.1. It is observed that the activation energy for α_c relaxation increases with increasing content of SnCCTO. This is due to increase in the stiffness of the composites with increasing content of SnCCTO.

It is also noted that in M" vs log f plots of PVDF and composites (Fig 7.6 c) that with ceramic dispersion M" peaks shift to low frequency, with increasing content of SnCCTO. This is because of the restriction in the movement of the polymer chains. Tensile test also confirms that with the increasing content of SnCCTO, composites become stiffer.

Table 7.1. Activation energy from M'' vs log f plots.

Sample	Activation Energy
SnCCTO	**0.67 eV**
PVDF	**0.70 eV**
PVDF-10SnC	**0.71 eV**
PVDF-20SnC	**0.78 eV**
PVDF-50SnC	**0.86 eV**

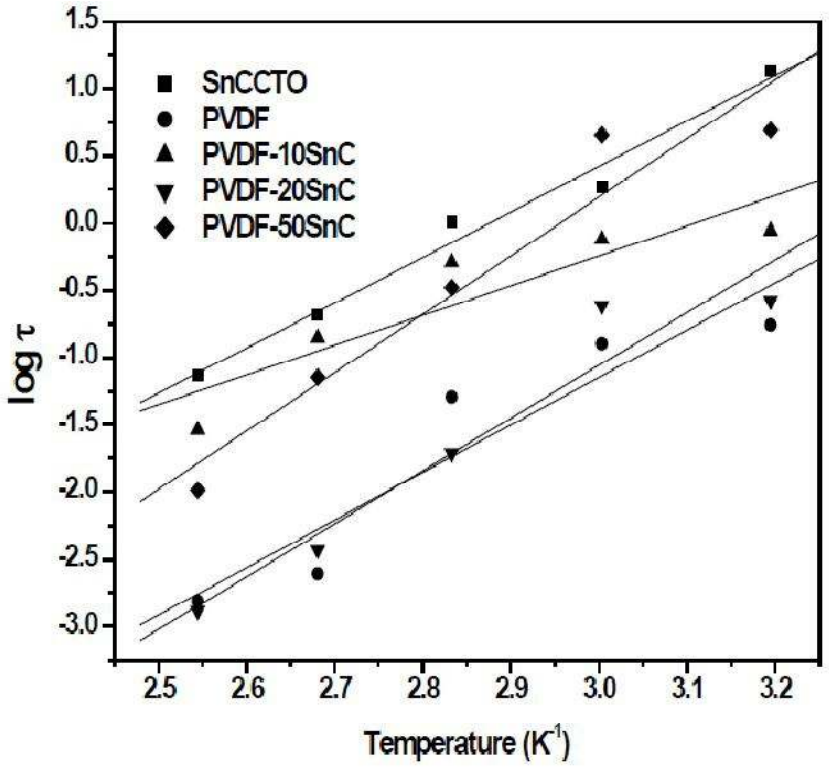

Figure 7.7 Log τ vs 1000/T curves for SnCCTO, PVDF, PVDF-10SnC, PVDF-20SnC and PVDF-50SnC.

To predict the effective dielectric permittivity (ε' or ε_{eff} are the same) of the composites, various models are used. The dielectric property of a diphasic dielectric mixture comprising of spherical crystallites with high dielectric permittivity and a matrix of low dielectric permittivity can be described by Maxwell's model [Maxwell 1954]. According to this model, the effective dielectric permittivity of the composite is given by

$$\varepsilon_{eff} = \frac{\delta_p \, \varepsilon_p \left(2/3 + \varepsilon_c/3\varepsilon_p\right) + \delta_c \, \varepsilon_c}{\delta_p \left(2/3 + \varepsilon_c/3\varepsilon_p\right) + \delta_c} \qquad (7.3)$$

where, ε_c, ε_p, δ_c and δ_p are the dielectric permittivity of CCTO, PVDF, the volume fraction of the ceramic and the polymer respectively. After substituting the values of ε_c, ε_p, δ_c and δ_p, the values of ε_{eff} obtained deviate much from the experimental values for all the volume fractions of SnCCTO under study (Fig 7.8).

In the case of Clausius-Mossotti model [Frolich 1949], it is assumed that the mixture of dielectric is composed of spherical crystallites dispersed in a continuous medium. The effective dielectric permittivity (ε_{eff}) of the composite is given by the following equation.

$$\varepsilon_{eff} = \varepsilon_p \left[1 + 3\delta \left(\frac{(\varepsilon_c - \varepsilon_p)}{\varepsilon_c + 2\varepsilon_p}\right)\right] \qquad (7.4)$$

The predicted value of ε_{eff} using this model also deviates a lot from the experimental values (Fig 7.8). This may be due to non spherical shape of SnCCTO particles as shown by SEM.

Lichtenecker's or logarithmic mixture rule is also used to predict the effective dielectric permittivity value [Nalwa 1995]. According to this model ε_{eff} is given by:

$$\text{Log}\, \varepsilon_{eff} = \delta_1 log\varepsilon_1 + \delta_2 log\varepsilon_2 \qquad (7.5)$$

Experimental results are significantly different from the predicted results using this model also (Fig 7.8). This is because Logarithmic law is applicable only when there is not much difference in the value of ε' of the dispersion medium and the dispersed phase. This is not true in the case of PVDF-SnC composites. Therefore the experimental results do not match exactly with the values predicted by these models.

The effective medium theory (EMT) model [Rao et al (2000] has been developed taking into account the morphology of the particles. According to this model, the ε_{eff} is given by

$$\varepsilon_{eff} = \varepsilon_p[1 + \frac{f_c(\varepsilon_c - \varepsilon_p)}{\varepsilon_p + n(1-f_c)(\varepsilon_c - \varepsilon_p)}] \qquad (7.6)$$

where f_c is the volume fraction of the ceramic dispersed, ε_c, ε_p and n are the dielectric permittivity of the ceramic, polymer and the ceramic morphology fitting factor respectively. The experimental values obtained are closest to the predicted values in this case of all the models employed to predict the ε_{eff} values. The shape parameter n has been found to be 0.012.

All these models have the limitations that the chemistry of the interfacial structure has not been taken into account and the particles are assumed to be of spherical shape. Microstructure and microchemistry of the interfaces are also very important to determine the physical, mechanical and electrical properties of the composites.

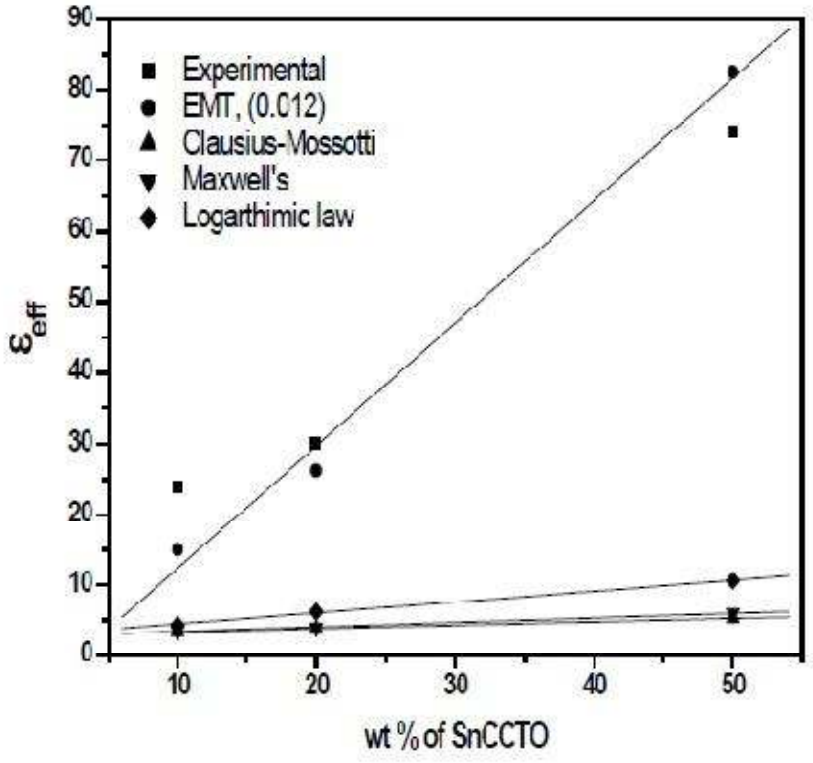

Figure 7.8 Variation of effective dielectric permittivity (ε_{eff}) measured at 100 Hz and 40^{o}C for PVDF-SnC composites based on various models.

Temperature-dependent dielectric relaxation is explained by Havriliak-Negami (H-N) function [Windlass et al (2001); Mijovic et al (2006)]:

$$\varepsilon^{*} = -i\frac{\sigma_{dc}}{\varepsilon_0 \omega^{s}} + \varepsilon_{\infty} + \sum_j \frac{(\Delta\varepsilon)_j}{[1+(iw\tau_j)^{\alpha}]^{\beta}} \qquad (7.7)$$

where, σ_{dc} is dc conductivity, ω is the angular frequency, s is an exponent ($0<s \leq 1$), τ_j is the relaxation time of the j^{th} process, ε_0 is the vacuum permittivity, $\Delta\varepsilon$ is the dielectric strength of the j^{th} process and α and β are the shape parameters of the H-N function which define the symmetric and asymmetric broadening of the α_c relaxation peak in ε'' curve. Analysis of H-N function using WinFit software program of PVDF and PVDF-50SnC composite have been given in Table 7.2 using deconvoluted H-N fits presented in (Fig.7.9). The exponent parameter, α represents the slope of the lower frequency side of

the relaxation peak in ε" curve. β is the asymmetry parameter which is calculated from the slope of higher frequency side of the same curve as α. The higher value of α for composites as compared to pure PVDF indicates a stretched relaxation over a wider range of frequencies whereas $0<\beta\leq1$ leads to asymmetrical broadening for the relaxation function. For β=1, the Debye-function is obtained. Asymmetry parameter β has a value of 1 for PVDF showing the symmetry of the spectrum. For the composites, β parameter has different values due to the dispersion of ceramics particles which creates heterogeneity in the system. For composites, the relaxation time (s) calculated from H-N fit decreases with increase in temperature. The composites exhibit lower relaxation time as compared to PVDF. Exact reason for this is not clear at present. With increase in the temperature, the relaxation time decreases in the composites. Lower value of relaxation time at higher temperature is because of the ease of relaxation at higher temperature due to increased mobility of the chains both for pure PVDF as well as composites.

Table 7.2 Fitting parameters for α_c relaxation as a function of temperature obtained from H-N fits.

Temp	PVDF, α	PVDF-50SnC, α	PVDF, β	PVDF-50SnC, β	PVDF, τ	PVDF-50SnC, τ
40^0C	0.49	0.61	1	0.57	2.33E-2	3.57E-3
80^0C	0.53	0.63	1	0.61	1.45E-3	7.71E-4
120^0C	0.57	0.74	1	0.70	7.44E-4	3.89E-5

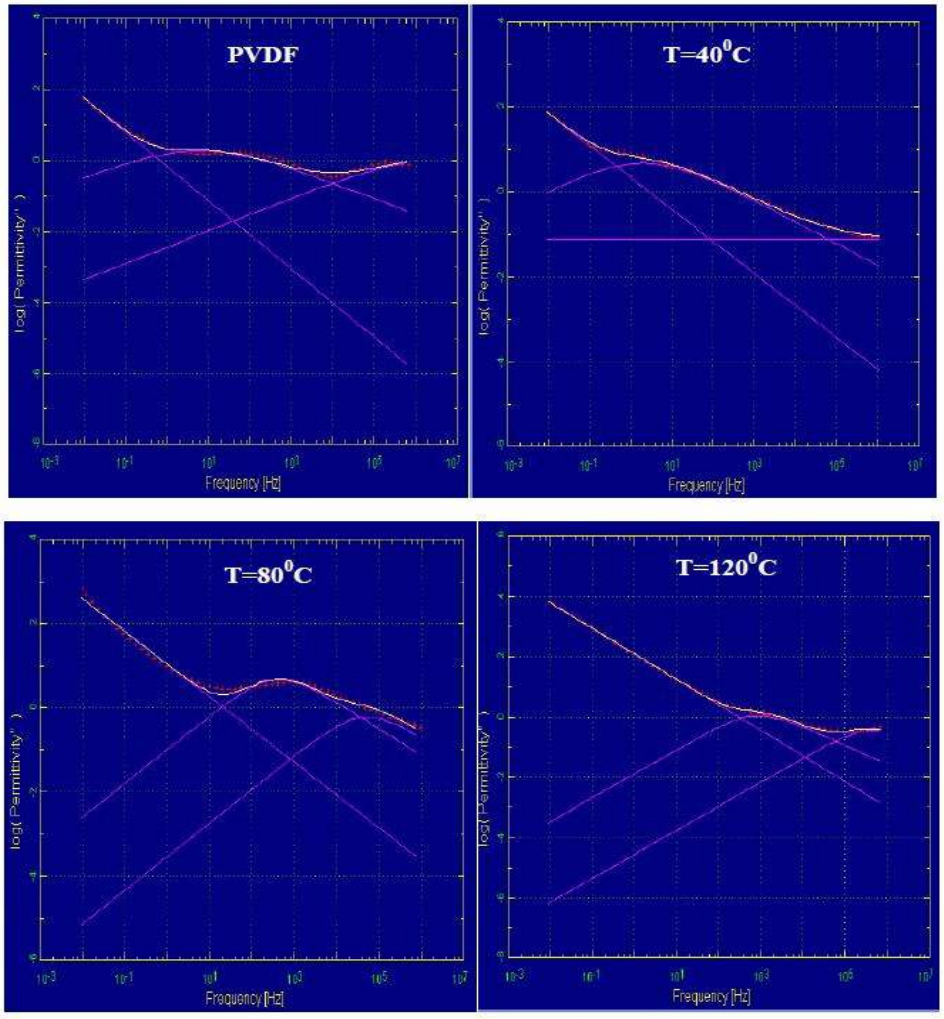

Figure 7.9 Dielectric loss in the frequency domain and spectrum was deconvoluted from H-N fits for PVDF-50SnC.

7.6. Conclusion

- $CaCu_3Ti_4O_{12}$ and Sn doped $CaCu_3Ti_4O_{12}$ (SnCCTO) have been synthesised by solid state ceramic method.

- Extrusion process was used to prepare the composites of PVDF and SnCCTO (PVDF-SnCCTO).

- XRD studies indicate no structural change in either polymer or ceramic in the composite.

- Young's modulus increases in the composites with increasing content of SnCCTO in PVDF.

- Dielectric permittivity of CCTO increases substantially with Sn doping accompanied by a slight increase in the dielectric loss. Dielectric permittivity increases with increase in SnCCTO in PVDF matrix. The values of dielectric permittivity obtained for the PVDF-50SnC sample in the present work is higher or at least comparable with the values of ε reported by most of the earlier workers at much lower volume fraction of SnCCTO in PVDF.

- In the composites, dielectric loss is slightly higher than that in the pure PVDF whereas it is less than that in SnCCTO.

- As the filler content increases in the PVDF matrix, the M' decreases. Two dielectric relaxations have been observed in the composites using modulus spectroscopy. One relaxation occurring at low frequency is of Maxwell-Wagner-Sillar (MWS) type, while the other relaxation occurring in the intermediate frequency range is due to α_c relaxation associated with molecular motion of the polymer chains in the crystalline regions of PVDF.

- Temperature dependence of the dielectric relaxation has been studied in details through H-N function. Debye type relaxation is observed in pure PVDF with $\beta=1$. Stretched relaxation over a wider range of frequency has been observed in the composites suggesting asymmetric nature of the relaxation.